Cell Research

www.nature.com/cr
www.cell-research.com

ARTICLE

CaMKIIα-driven, phosphatase-checked postsynaptic plasticity via phase separation

Qixu Cai[1], Menglong Zeng[1,2], Xiandeng Wu[1], Haowei Wu[1], Yumeng Zhan[1], Ruijun Tian[3] and Mingjie Zhang[1,4]

Ca^{2+}/calmodulin-dependent kinase IIα (CaMKIIα) is essential for synaptic plasticity and learning by decoding synaptic Ca^{2+} oscillations. Despite decades of extensive research, new mechanisms underlying CaMKIIα's function in synapses are still being discovered. Here, we discover that Shank3 is a specific binding partner for autoinhibited CaMKIIα. We demonstrate that Shank3 and GluN2B, via combined actions of Ca^{2+} and phosphatases, reciprocally bind to CaMKIIα. Under basal condition, CaMKIIα is recruited to the Shank3 subcompartment of postsynaptic density (PSD) via phase separation. Rise of Ca^{2+} concentration induces GluN2B-mediated recruitment of active CaMKIIα and formation of the CaMKIIα/GluN2B/PSD-95 condensates, which are autonomously dispersed upon Ca^{2+} removal. Protein phosphatases control the Ca^{2+}-dependent shuttling of CaMKIIα between the two PSD subcompartments and PSD condensate formation. Activation of CaMKIIα further enlarges the PSD assembly and induces structural LTP. Thus, Ca^{2+}-induced and phosphatase-checked shuttling of CaMKIIα between distinct PSD nano-domains can regulate phase separation-mediated PSD assembly and synaptic plasticity.

Cell Research (2020) 0:1–15; https://doi.org/10.1038/s41422-020-00439-9

INTRODUCTION

Synaptic plasticity underlies the cellular basis of learning and memory. Taking hippocampal CA1 pyramidal neuron as an example, high frequency stimulation-induced synaptic Ca^{2+} influx via NMDA receptors (NMDAR) activates Ca^{2+}/calmodulin-dependent kinase II (CaMKII) and initiates downstream signaling events. The outcome of the stimulation is long-term synaptic physiological and structural changes including elevated AMPA receptors (AMPAR) numbers in the postsynaptic sites, enlarged dendritic spine volumes and expanded postsynaptic density (PSD) sizes.[1–4]

PSDs are mega-protein assemblies enriched in scaffold protein, glutamate receptors, synaptic adhesion molecules and signaling molecules. PSDs in excitatory synapses form layered structures. The top layer of PSD, which is within 30–40 nm to the postsynaptic membrane, contains the MAGUK family scaffold proteins (e.g., PSD-95) that directly bind to both NMDAR and AMPAR embedded in synaptic membranes. The lower layer of PSD, which is from ~40 to ~100 nm measured from the postsynaptic membrane, contains scaffold proteins including Shank and Homer, which further associate with the actin cytoskeleton facing spine cytoplasm.[5,6] These two layers are interconnected by another scaffold protein called SAPAP (aka GKAP and DLGAP). When stimulated, a synapse can significantly enlarge its volume at least partly due to accumulation of the PSD scaffold proteins.[7–9] The size of PSD is linearly correlated with the electric strength of the synapse as larger PSDs contain more AMPARs anchored to the postsynaptic membranes.[10,11] We recently have provided evidences showing that formation of the dense PSD assemblies are driven by specific and multivalent interactions among major PSD scaffold proteins and their binding partners via liquid–liquid phase separation (LLPS).[12–14] Phase separation-mediated formation of PSD condensates provides a new angle to interpret numerous observations accumulated in the past decades of research in synaptic biology. The reconstitution of a simplified version of PSD may offer unique opportunities to investigate synapse formation and plasticity, as the complex and variable shapes of synapses pose practical challenges in elucidating molecular mechanisms governing synaptic plasticity.[15]

CaMKII, one of the most abundant protein in PSD, and is responsible for decoding synaptic Ca^{2+} signal and crucial for synaptic plasticity.[1–4] Upon stimulation, CaMKII undergoes rapid translocation from cytoplasm to the activated dendritic spine, which is followed by sustained increase of the major scaffold proteins including PSD-95, SAPAP, Shank and Homer as well as enlargement of the spine volume and thickening of PSD.[7–9,16–18] Advancement in super-resolution imaging revealed sub-synaptic molecular organizations that are critical for synaptic function. Formation of distinct synaptic scaffold nano-domains together with glutamate receptors is being recognized as an effective mechanism for synaptic transmission modulation.[19–21] Electron microscopy (EM) studies also showed that, within the PSD of an activated synapse, there are two populations of CaMKII: one is very close to the postsynaptic membrane and presumably corresponds to the NMDAR-bound form of the enzyme; the other is in the lower layer of PSD overlapping with the Shank and Homer scaffolds ([22] and refs therein). These EM studies suggest that, in addition to translocating from spine cytoplasm to PSD, CaMKII can also shuttle between distinct subcompartments (or nano-domains) within PSD

[1]Division of Life Science, State Key Laboratory of Molecular Neuroscience, Hong Kong University of Science and Technology, Clear Water Bay, Kowloon, Hong Kong, China; [2]McGovern Institute for Brain Research, Department of Brain and Cognitive Sciences, Massachusetts Institute of Technology, Cambridge, MA 02139, USA; [3]Department of Chemistry, Southern University of Science and Technology, Shenzhen, Guangdong 518055, China and [4]Center of Systems Biology and Human Health, Hong Kong University of Science and Technology, Clear Water Bay, Kowloon, Hong Kong, China
Correspondence: Mingjie Zhang (mzhang@ust.hk)

Received: 12 September 2020 Accepted: 27 October 2020
Published online: 24 November 2020

(i.e., the top and lower layers of PSD). However, currently there is no technology available to investigate how CaMKII can move between different subcompartments and what the functions of the enzymes are in these different subcompartments of synapses in living neurons due to the resolution limit of optical imaging.

In this study, we discover that Shank3, using its N-terminal domain-ankyrin repeats (NTD-ANK) tandem, specifically interacts with CaMKIIα. Importantly, Shank3 NTD-ANK only binds to the basal state of CaMKIIα (i.e., the autoinhibited state of the enzyme under basal condition). Using a reconstituted PSD, we demonstrate that inactive CaMKIIα is enriched in the Shank3 subcompartment of PSD. Upon stimulation, the active CaMKIIα shuttles to the GluN2B subcompartment via direct interaction between GluN2B and CaMKIIα. Interestingly, inactivation of CaMKIIα by protein phosphatases shuttles the enzymes back to the Shank3 subcompartment. The shuttling of CaMKIIα between the two PSD subcompartments is modulated by Ca^{2+} concentration oscillations and guarded by phosphatases. Ca^{2+}-induced activation of CaMKIIα further enlarges the PSD assembly. Our findings explain how distinct nano-domains in PSD might form and suggest an activity-dependent CaMKII inter-subcompartment shuttling mechanism that may underlie different forms of synaptic plasticity.

RESULTS

Identification of CaMKII as a specific binder of the Shank3 NTD-ANK tandem

Shank3 N-terminus contains an NTD-ANK tandem but its function remains largely elusive (Fig. 1a). To identify its potential binding proteins, we performed an affinity purification using purified GST-tagged Shank3 NTD-ANK tandem as the bait, with GST tag alone or GST-Shank3 SH3-PDZ domain as the specificity controls, using rat brain lysates (Fig. 1b). Mass spectrometry analysis showed that CaMKIIα was ranked as the top binding partner for GST-Shank3 NTD-ANK. In contrast, the control baits showed little or no recognition of CaMKII (Fig. 1b), suggesting a highly specific interaction between Shank3 NTD-ANK and CaMKII in rodent brains. Note that our affinity purification was performed under the Ca^{2+}-free condition in all purification steps, suggesting that Shank3 NTD-ANK binds to autoinhibited CaMKII (see below for more details). This contrasts with a recent finding that an unstructured fragment of Shank3 in the middle of the protein (aa 931–1014) binds to T286-autophosphorylated CaMKII.[23]

CaMKIIα specifically binds to Shank3 NTD-ANK

CaMKII consists of a kinase domain, an autoinhibitory segment (AIS), a linker region and a hub domain (abbreviated as "K-A-L-H"; Fig. 1a). Pull-down experiments showed that GST-Shank3 NTD-ANK binds to full-length CaMKIIα expressed in HEK293T cells (Fig. 1c). None of the tested fragments of CaMKIIα showed detectable binding to NTD-ANK (Supplementary information, Fig. S1a), indicating that Shank3 only binds to the full-length CaMKIIα. The kinase dead mutant CaMKIIα-D135N bound to Shank3 as effectively as the wide-type (WT) kinase did (Supplementary information, Fig. S1a), thus the kinase activity is not required for the interaction. Neither CaMKIIα-T286D nor CaMKIIα-T286E showed detectable binding to Shank3 NTD-ANK (Fig. 1c), suggesting that the interaction between CaMKIIα and Shank3 depends on the conformational status of CaMKIIα.

CaMKIIα and β are highly similar (91% amino acid sequence identity in their kinase and autoinhibitory segment) and both are enriched in PSD. The GST pull-down experiments showed that Shank3 only binds to CaMKIIα but not to β (Fig. 1d, lanes 1 and 2). Using domain swapped CaMKIIα/β chimeras, we found that the kinase domain and the autoinhibitory segment of CaMKIIα are essential for Shank3 binding, as the CaMKIIα chimeras with the "Kinase + AIS" segments from CaMKIIβ failed to bind to Shank3 NTD-ANK (Fig. 1d, lanes 3 and 4). The hub domain does not play a role in the binding specificity (Fig. 1d, lanes 5 and 6). Interestingly, the CaMKIIα chimera with the longer CaMKIIβ "Linker" slightly but significantly weakened the binding (Fig. 1d, lane 7). Additional mapping revealed that two residues in the last helix (i.e., α10) of the CaMKIIα kinase domain (S272 and H273), which are totally conserved in CaMKIIα but are not in CaMKIIβ/γ/δ (Fig. 1e), to be essential for the binding (Fig. 1d, lane 9). However, replacing C273 and Q274 on CaMKIIβ with "SH" did not convert CaMKIIβ into a Shank3 binder, indicating that regions outside α10 are also required (Fig. 1d, lane 10). The Shank3 NTD-ANK affinity purification recovered CaMKIIβ, γ and δ were likely due to incorporation of these isoforms into the CaMKII dodecameric holoenzyme. Finally, Neither NTD nor ANK had detectable binding to CaMKIIα, indicating that the NTD-ANK tandem is required for the binding (Supplementary information, Fig. S1b).

Structural model of the Shank3 NTD-ANK/CaMKIIα complex

Several autism spectrum disorder-associated missense mutations have been identified in Shank3 NTD-ANK[24–26] (Fig. 1a). One of these mutations, R12C, significantly weakened its binding to CaMKIIα. Substitution of R12 with Glu or Ala essentially abolished the binding (Fig. 2a). Further mapping discovered that the linker connecting NTD and ANK is also essential for the binding, as substitution of I102 in the linker with Ala abolished the (Fig. 2b). Structural analysis showed that both R12 and I102 are on the same face of the Shank3 NTD-ANK tandem (Supplementary information, Fig. S1c).

The residues identified above were used as ambiguous distance restraints for docking of the Shank3 NTD-ANK structure to a single subunit in the autoinhibited conformation of CaMKIIα[27] using HADDOCK2.2.[28] We were able to obtain highly converged structural models of the CaMKIIα/Shank3 NTD-ANK complex in the docking calculations (Fig. 2c, d). In this docked complex model, NTD and the linker between NTD and ANK are in contact with the backside (relative to the T- and S-sites) of the C-lobe of the CaMKIIα kinase domain (Fig. 2c, d). S272 and H273 are in proximity with the NTD and ANK linker. Y106 and E105 from the N-lobe of CaMKIIα are within the distance range to form cation-π or electrostatic interaction with R12 of Shank3 (Fig. 2d). We validated this structural model using site-directed mutagenesis. Substitution of $Y106_{CaMKIIα}$ with Ala abolished the binding but substitution of $E105_{CaMKIIα}$ with Ala had no impact (Fig. 2e). Based on the CaMKIIα/Shank3 NTD-ANK structural model, we constructed another structural model of the fully closed dodecameric CaMKIIα[27,29] in complex with Shank3 NTD-ANK (Fig. 2f). In the complex, Shank3 NTD-ANK binds to the solvent-exposed surface of the CaMKIIα kinase domain. There is no steric hinderance between CaMKIIα and Shank3 NTD-ANK, even when the kinase is in the most compact state (Supplementary information, Fig. S1d).

Shank3 NTD-ANK binds to autoinhibited CaMKIIα

CaMKIIα adopts multiple conformations in response to various stimulations. Each conformational state is with a different level of kinase activity and distinct target binding property.[3,4] All GST pull-down experiments shown in Figs. 1 and 2 were performed under the Ca^{2+}-free condition. Under such condition, the autonomy-mimicking mutant (T286D or T286E) prevented CaMKIIα from binding to Shank3 (Fig. 1c), indicating that Shank3 NTD-ANK only binds to CaMKIIα adopting the autoinhibited conformation.

The Ca^{2+}-CaM-bound form of CaMKIIα retained its binding to Shank3 NTD-ANK (Fig. 3a). Further addition of Mg^{2+}-ATP disrupted the interaction, presumably due to autophosphorylation of CaMKIIα (Figs. 3a and 1c). The T305E and T306E double mutation of CaMKIIα (termed T305/6E) retained its binding to Shank3 NTD-ANK even in the presence of ATP, as the mutant could not be activated by Ca^{2+}-CaM (Fig. 3a). The kinase dead mutant CaMKIIα-D135N and the T286-autophosphorylation-deficient mutant

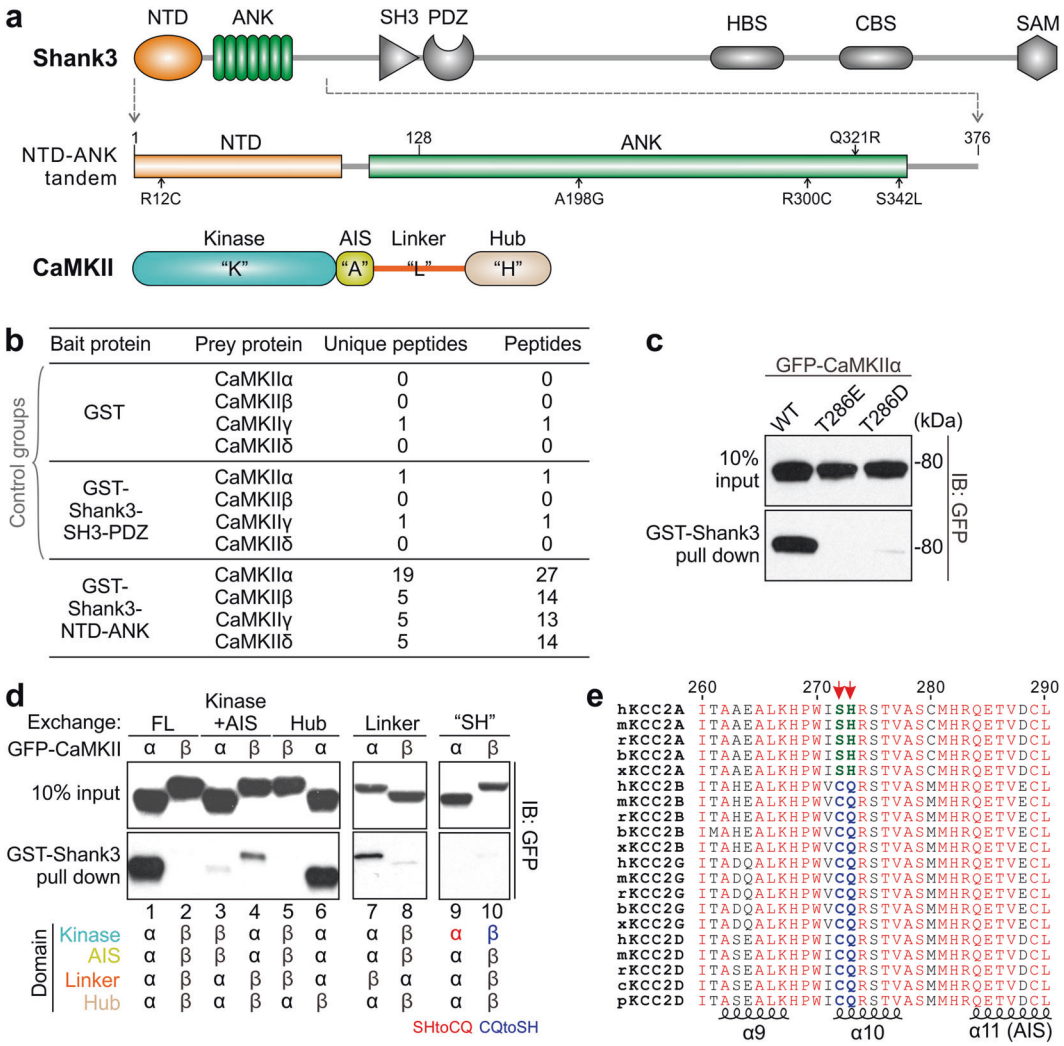

Fig. 1 The NTD-ANK tandem of Shank3 specifically binds to CaMKIIα. a Schematic diagram showing the domain organization of Shank3 and CaMKII. Several missense variants in the Shank3 NTD-ANK tandem identified in patients are indicated. **b** Mass spectrometry results of the affinity purifications. Only Shank3 NTD-ANK specifically binds purified CaMKII. The purification was repeated multiple times with essentially the same results. **c** Substitution of T286 in CaMKIIα with either Asp or Glu abolished its Shank3 binding. **d** Characterization of the bindings of GST-Shank3 NTD-ANK to CaMKIIα, CaMKIIβ, or chimeras with different combinations of the two isozymes domains as indicated at the bottom of the panel. For an example, the CaMKII chimera in lane 3 (labeled as "ββαα") is composed of the kinase domain, the AIS domain of CaMKIIβ, the linker and hub domains of CaMKIIα. In lane 9, the "SH" cassette of CaMKIIα was replaced by the corresponding "CQ" cassette from CaMKIIβ. In lane 10, the "CQ" cassette from CaMKIIβ was replaced by the "SH" cassette of CaMKIIα. **e** Amino acid sequence alignment of the α10 and the following AIS segment of different isoforms of CaMKII ("h" for human; "m" for mouse; "r" for rabbit; "b" for bovine; "x" for xenopus; "c" for chicken; "p" for pig) showing that the "SH" cassette is unique to CaMKIIα. The secondary structure is based on the crystal structure of CaMKIIα holoenzyme (PDB ID: 3SOA).

CaMKIIα-T286A both bound to Shank3 under all assay conditions (Fig. 3a). Taken together, the above results revealed that, as long as T286 is not phosphorylated (i.e., when the enzyme is in the autoinhibited conformation), CaMKIIα can robustly bind to Shank3 (Fig. 3g). The results further indicated that T286 phosphorylation-induced disruption of the interaction between CaMKIIα and Shank3 is likely due to the release of autoinhibitory segment from the kinase domain.[30] In the presence of Ca^{2+}-CaM but without ATP, a condition that does not really exist in synapses of living neurons, the α11 region in the autoinhibitory segment of CaMKII adopts a more flexible conformation but remaining partially autoinhibited[31] and the enzyme can still bind to Shank3. However, in synapses, T286 is rapidly autophosphorylated once the enzyme is bound to Ca^{2+}-CaM. Thus, the Ca^{2+}-CaM-bound but T286 unphosphorylated CaMKII is a very transient state but can be stably trapped in vitro (indicated as the "Priming" state in Fig. 3g).

Reciprocal binding of Shank3 and GluN2B to CaMKIIα

NMDA receptor subunit GluN2B binds to the T-site of CaMKIIα,[32] which is available only when the autoinhibitory segment is released. Thus, Shank3 and GluN2B appear to bind to CaMKIIα in distinct conformational states. We designed a series of GST pull-down assay to capture different conformational states of CaMKIIα (Fig. 3b). In condition 1, both incubation buffer and washing buffer contained EGTA, and CaMKIIα was in the fully autoinhibited conformation. In condition 2, Ca^{2+}-CaM was present in both incubation buffer and washing buffer. CaMKIIα was in Ca^{2+}-CaM bound but unphosphorylated state with partial opening of its autoinhibitory segment.[31] In condition 3, Ca^{2+}-CaM was present in the incubation buffer and EGTA was in the washing buffer, and CaMKIIα should be back to the totally autoinhibited state. In conditions 4–6, both Mg^{2+}-ATP and Ca^{2+}-CaM were present in the incubation buffer, allowing autophosphorylation to occur. In

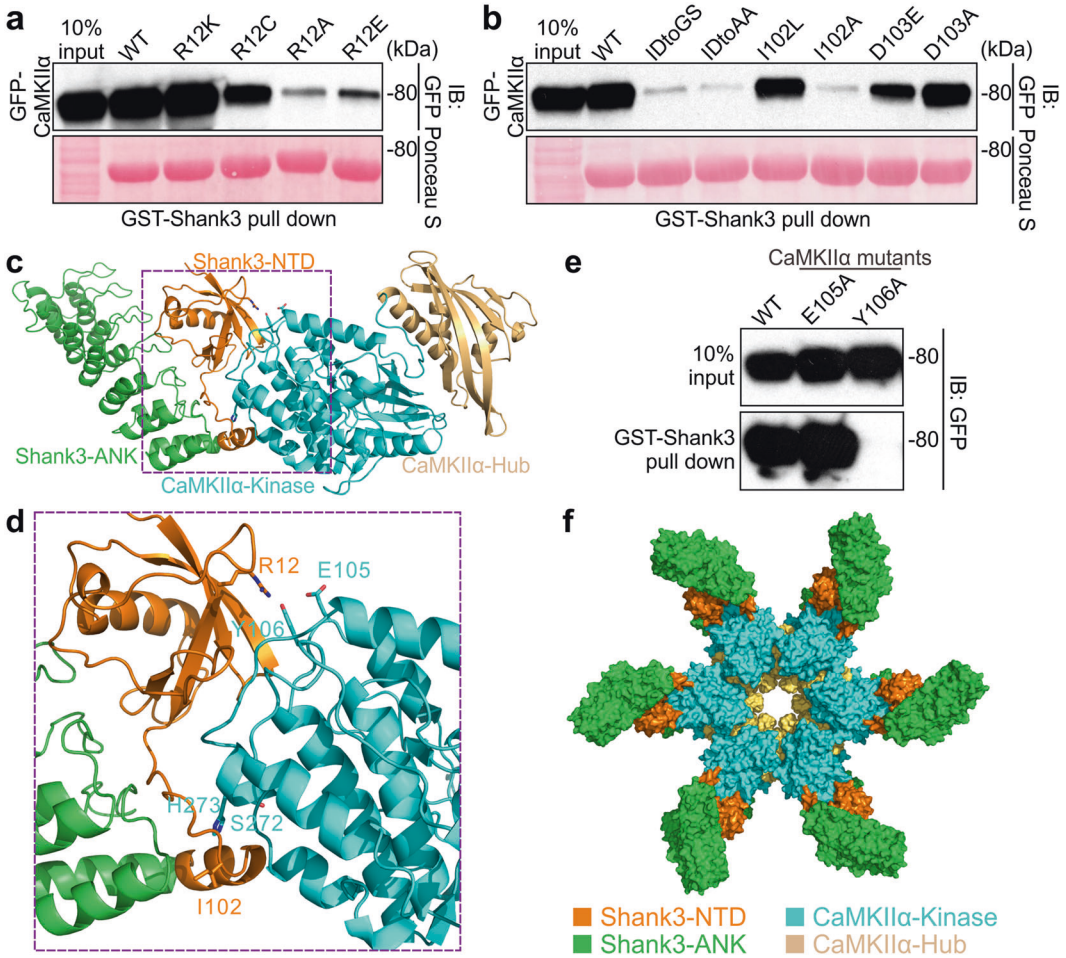

Fig. 2 Structural model of the Shank3 NTD-ANK/CaMKIIα complex. a Substitutions of R12 of Shank3 NTD-ANK with different amino acid residues have different impact on its binding to CaMKIIα. **b** The region containing I102 and D103 in Shank3 NTD-ANK is critical for CaMKIIα binding. **c** A structural model of the Shank3 NTD-ANK and CaMKIIα complex derived from the experimental restraints-based docking calculations. **d** A zoomed-in region showing the binding interface between Shank3 NTD-ANK and CaMKIIα. The model shows that R12 from Shank3 interact with Y106 and possibly with E105 from CaMKIIα. **e** Experimental validation showing that substitution Y106 with Ala abolished CaMKIIα's binding to Shank3 NTD-ANK. **f** A structural model showing Shank3 NTD-ANK binding to the autoinhibited, dodecameric CaMKIIα.

condition 4, Ca^{2+} was also included in washing buffer so CaMKIIα was fully activated. Conditions 5 and 6 were the same as in condition 4 except that EGTA was included in the washing buffer, so CaMKIIα was expected to be in autonomy state (i.e., T286, T305/306 phosphorylated but Ca^{2+}-CaM dissociated)[33,34] (also see Fig. 3g). The difference between condition 5 and 6 was the time point of EGTA treatment. In condition 6, EGTA was added after autophosphorylation and before adding GST-Shank3 or GST-GluN2B.

Purified GST-tagged GluN2B fragment (aa 1259–1310, termed GST-GluN2B) and HEK293T cell lysate containing overexpressed GFP-CaMKIIα were used for the GST pull-down assay. Consistent with the earlier finding,[32] GST-GluN2B showed strongest binding to the fully activated CaMKIIα (condition 4 in Fig. 3c; note that a prominent CaMKIIα band was detected in ponceau S staining). Removal of Ca^{2+}-CaM during washing led to only slight weakening of the binding (condition 5 in Fig. 3c). The Ca^{2+}-CaM-bound but not autophosphorylated CaMKIIα also showed weak binding to GluN2B (condition 2 in Fig. 3c). Unexpectedly, GST-GluN2B did not bind to GFP-CaMKIIα in condition 6 (Fig. 3c), in which CaMKIIα was expected to be in the autonomy form as in condition 5. The above result hinted that certain factor(s) in the HEK293T cell lysate could abolish the GluN2B/CaMKIIα interaction when EGTA was added to the binding mixture before GST-GluN2B.

We repeated the pull-down assay using purified CaMKIIα, the outcome totally matched with the original prediction (Fig. 3d). Specifically, the bindings of GluN2B to CaMKIIα in conditions 5 and 6 were the same and slightly weaker than in condition 4 (Fig. 3d), further supporting that certain factor(s) in the HEK293T cell lysates can prevent CaMKIIα from binding to GluN2B.

To directly test this hypothesis, we compared the bindings of GST-Shank3 and GST-GluN2B to purified CaMKIIα with and without addition of HEK293T cell lysate (500 μg total protein from lysate for each reaction, Fig. 3e). GST-Shank3 bound to CaMKIIα under conditions 1–3 both with and without presence of HEK293T cell lysate (Fig. 3e). Addition of HEK293T cell lysate in condition 6 eliminated the GluN2B/CaMKIIα interaction and concomitantly restored the Shank3/CaMKIIα interaction (Fig. 3e). We checked the autophosphorylation status of CaMKIIα in each reaction condition. Without cell lysate, the autophosphrylation of CaMKIIα totally fit with our original prediction: no autophosphorylation for conditions 1–3, T286 highly phosphorylated in conditions 4–6, and T305 (likely T306 as well) phosphorylated only in conditions 5–6. Remarkably, with the presence of cell lysate, the autophosphorylations of CaMKIIα at both T286 and T305 were greatly reduced. T286 phosphorylation was eliminated in condition 6 (Fig. 3e).

Further enzymology studies, pharmacological manipulations, and biochemical purifications allowed us to firmly establish that

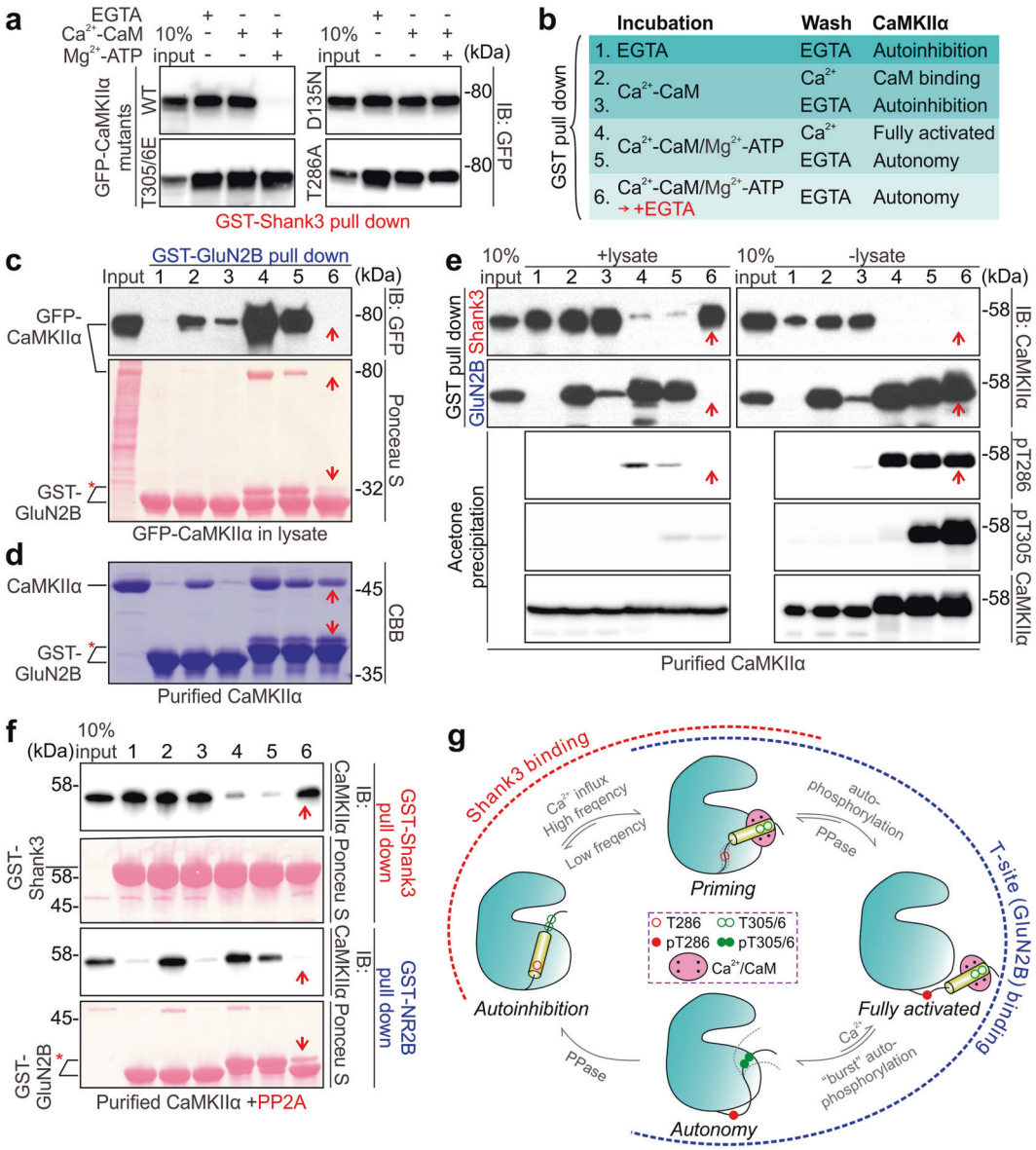

Fig. 3 Reciprocal binding of Shank3 and GluN2B to CaMKIIα. a GST-Shank3 pull-down experiments using various mutants of CaMKIIα indicating that binding of Ca^{2+}-CaM does not disrupt the Shank3 interaction of CaMKIIα, whereas T286 autophosphorylation abolishes CaMKIIα's binding to Shank3. **b** Table illustrating six different conditions for the GST pull-down experiments. All buffers were based on TBS buffer with 5 mM DTT. The concentration of EGTA or $CaCl_2$ was 1 mM. The $MgCl_2$ concentration was 10 mM. The ATP concentration was 0.5 mM. The CaM concentration was 3 μM. The conformations and activities of CaMKIIα under each condition are also indicated. **c-d** GST-GluN2B pull-down experiment using HEK293T cells lysates containing expressed GFP-CaMKIIα (**c**) or CaMKIIα expressed in and purified from bacteria (**d**), showing the bindings between GluN2B and CaMKIIα under different conditions. Note the opposite binding outcomes in condition 6 (highlighted by red arrows) when using CaMKIIα from cell lysates (**c**) or the purified enzyme (**d**). The red asterisks indicate the up-shifted, phosphorylated GST-GluN2B. **e** GST-Shank3 and GST-GluN2B pull-down results using purified CaMKIIα with or without adding HEK293T cell lysates, showing the reciprocal binding of Shank3 and GluN2B to CaMKIIα. In parallel sets of experiments, CaMKIIα was precipitated from each reaction mixture by acetone and their phosphorylation states were probed by specific antibodies. CaMKIIα probed by the monoclonal antibody (6G9) displayed significantly up-shifted and stronger bands in conditions 4–6 in the absence of lysate due to the conformation-specificity of the antibody.[62] **f** The results of the GST-Shank3 and GST-GluN2B pull-down assays using purified CaMKIIα and in the present of purified PP2A (10 nM). The results under conditions 6 are highlighted by red arrows. The red asterisk indicates the phosphorylated GST-GluN2B. **g** Schematic diagram showing the activity states of CaMKIIα and its corresponding binding capacity to Shank3 and GluN2B.

phosphatases (PP2A and likely PP1 as well) in HEK293T cell lysate can effectively dephosphorylate CaMKIIα and modulate its binding to GluN2B and Shank3 (Supplementary information, Fig. S2 and additional text of the Figure for details). We further showed that purified PP2A could effectively block the GluN2B/CaMKIIα interaction and concomitantly restore the Shank3/CaMKIIα binding (condition 6, Fig. 3f).

Taken together, we discovered that Shank3 and GluN2B can reciprocally bind to CaMKIIα. Shank3 can interact with the fully autoinhibited or the Ca^{2+}-CaM-bound but unphosphorylated CaMKIIα. Ca^{2+}-CaM binding partially opens the T-site of the enzyme and allow the binding of GluN2B. T286 phosphorylation dramatically enhances GluN2B's binding to CaMKIIα. PP2A and likely PP1 as well can rapidly dephosphorylate CaMKIIα when the

Ca^{2+} concentration becomes low and dephosphorylated CaMKIIα can bind to Shank3. It is known that both PP2A and PP1 are enriched in neuronal synapses.[35,36] Thus, the balance between Ca^{2+}-induced autophosphorylation and specific phosphatase-mediated dephosphorylation can tune the conformation, catalytic activity and target binding property of CaMKIIα (Fig. 3g).

Recruitment of CaMKIIα to Shank3 condensates through direct interaction

Based on our previously studies,[13,37] we generated a simplified version of Shank3, which contained the NTD-ANK tandem, the extended PDZ domain, the Homer binding sequence (HBS), the cortactin binding sequence (CBS) and the C-terminal SAM domain. An N-terminal GB1 tag and three point mutations (L231R and F304Y in ANK and M1718A in the SAM domain) were combined to improve the protein solubility.[13,37] This version of Shank3 contains known target binding domains/motifs and lacks most of the unstructured regions (Supplementary information, Fig. S3a, referred to as Shank3 from here on) as well as the previously identified active CaMKIIα binding site in the middle of the protein.[23]

The recombinant Shank3 was purified in high salt buffer containing 500 mM NaCl with good solubility. Once exchanged into low salt buffer, the protein formed numerous spherical droplets, indicating Shank3 itself underwent phase separation in low salt buffers at concentration ~1 μM or above (Supplementary information, Fig. S3b, c and e). Fluorescence recovery after photobleaching (FRAP) assay indicated that Shank3 in the condensed droplets could exchange with those in the diluted solution (Supplementary information, Fig. S3d). CaMKIIα alone did not undergo LLPS at the concentration as high as 100 μM tested (data not shown).

Differential interference contrast (DIC) and fluorescence images showed that CaMKIIα was enriched into Shank3 condensed droplets (Fig. 4a), a process which was also sensitive to salt concentrations in the buffer (Supplementary information, Fig. S3f). FRAP assay revealed that the signal recovery for Shank3 and less so for CaMKIIα (Fig. 4b; Supplementary information, Fig. S3g). Time-lapse imaging showed that the Shank3/CaMKIIα condensed droplets could fuse with each other (Fig. 4c). Imaging- and sedimentation-based experiments showed Shank3 and CaMKIIα could undergo LLPS at the concentration below 1 μM (Fig. 4a, d).

We tested the impact of individual Shank3 point mutations (R12K, R12C, R12A, R12E, and I102A, Fig. 2a, b) on the phase separation of Shank3/CaMKIIα. In parallel with their gradual weakening in binding to CaMKIIα when $R12_{Shank3}$ was mutated (Fig. 2a), the enrichments of CaMKIIα in the Shank3 condensates were also gradually reduced (Fig. 4e, f). $I102A_{Shank3}$ and $SHtoCQ_{CaMKIIα}$ mutations that could disrupt the Shank3/CaMKIIα interaction also prevented CaMKIIα to be enriched in the Shank3 condensates (Fig. 4e, f). As the control, none of the Shank3 mutations tested had obvious impact on its condensate formation (Supplementary information, Fig. S3h, i). Taken together, we conclude that inactive CaMKIIα can be recruited to and enriched in the Shank3 condensates through the direct binding.

GluN2B disperses the CaMKIIα/Shank3 condensates in the presence of Ca^{2+}

CaMKIIα is reversibly translocated from cytosol to PSD upon NMDA receptor activation-induced Ca^{2+} influx.[16] The anchoring of CaMKIIα in PSD is mediated by the direct binding of the enzyme to GluN2B.[32] The CaMKII binding sequence of GluN2B is located in the C-terminal cytosolic tail of GluN2B and is homologous to the sequence surrounding T286 of CaMKIIα (Supplementary information, Fig. S4a). A peptide containing the CaMKIIα binding sequence of GluN2B (aa 1289–1310, GluN2Bpep) interacted with CaMKIIα/Ca^{2+}-CaM (aa 1–314 for CaMKIIα) with a K_d of ~0.33 μM (Supplementary information, Fig. S4b).

Since Shank3 and GluN2B reciprocally bind to CaMKIIα (Fig. 3g), one would expect that increase of Ca^{2+} concentration would switch CaMKIIα to bind to GluN2B, and thus disperse the Shank3/CaMKIIα condensates. DIC and fluorescence imaging experiments indeed showed that, in the presence of GluN2Bpep, addition of Ca^{2+}-CaM dispersed CaMKIIα from the Shank3 condensates in a time-dependent manner (Fig. 4g; Supplementary information, Movie S1). The sedimentation-based assay showed that nearly all CaMKIIα was dispersed from the Shank3 condensates when Ca^{2+}-CaM was added (Fig. 4h). Thus, in the presence of Ca^{2+}-CaM (i.e., under the NMDAR stimulated condition in synapses) GluN2B can form a stable GluN2B/Ca^{2+}-CaM/CaMKIIα complex (Fig. 3g). The interaction between Shank3 and CaMKIIα under low Ca^{2+} concentration condition may allow rapid shift of a portion of CaMKIIα "stored" by Shank3 to NMDAR upon synapse activation.

GluN2B recruits activated CaMKIIα into the GluN2B/PSD-95 condensates

NMDARs form very large molecular assemblies with PSD-95 in PSDs.[38] PDZ binding motif (PBM) of GluN2B can interact with the PDZ domains of PSD-95 to promote LLPS of PSD-95 in the PSD condensates.[13,39,40] Mixing purified GluN2B (aa 1170–1482; Supplementary information, Fig. S4a) with the full-length PSD-95 led to phase separation of the complex (Supplementary information, Fig. S4c, d). Next, we asked whether activated CaMKIIα might be recruited to the GluN2B/PSD-95 condensates via GluN2B-mediated binding.

When PSD-95, GluN2B and CaMKIIα were mixed in the presence of Ca^{2+}-CaM, the three proteins readily formed condensed droplets at the protein concentration as low as ~1 μM (Fig. 5a; Supplementary information, Fig. S4e). The FRAP assays indicated that both PSD-95 and GluN2B in the droplets constantly exchanged with molecules in the diluted solution (Supplementary information, Fig. S4f). Removal of the PBM from GluN2B (deleting aa 1478–1482, termed ΔPBM) significantly decreased PSD-95 to be enriched to the GluN2B and CaMKIIα (Fig. 5b). The I205K mutation of CaMKIIα, which disrupts the enzyme's T-site coupling as well as GluN2B binding,[32] totally prevented CaMKIIα from being enriched into the GluN2B/PSD-95 condensates and the level of GluN2B and PSD-95 in the condensed phase became comparable to the simple mixture of the two proteins only (Fig. 5b). Thus, the formation of the PSD-95, GluN2B and CaMKIIα condensates in the presence of Ca^{2+}-CaM requires specific pairwise interactions among the three proteins.

Ca^{2+} oscillation-modulated upper layer PSD assembly formation

The data in Fig. 3 show that the activated CaMKIIα effectively binds to GluN2B, but such binding can be quickly reversed by phosphatases such as PP2A when Ca^{2+} is removed in the mixture. This immediately suggests that, in the presence of phosphatases, the formation of the PSD-95, GluN2B and CaMKIIα condensates may be directly regulated by the Ca^{2+} concentration oscillations. To recapitulate such Ca^{2+}-dependent reversible PSD-95, GluN2B and CaMKIIα condensate formation, we set up three assay conditions: the first condition mimicked the basal synaptic activity with CaM, CaMKIIα, PSD-95, GluN2B, and PP2A mixed in the presence of EGTA and Mg^{2+}-ATP ("Basal" in Fig. 5c); the second condition corresponded to the synapse stimulated condition with Ca^{2+} added to the "Basal" condition mixture ("Stim" in Fig. 5c); the third condition modeled synaptic Ca^{2+} concentration decrease by a time-delayed addition of EGTA to the "Stim" condition (termed "Basal" in Fig. 5c). The time delayed addition of EGTA in the third condition would allow dephosphorylation of CaMKIIα by PP2A due to CaM dissociation and convert the system back to the basal synaptic condition.

The DIC and fluorescence imaging assays showed that there was nearly no CaMKIIα enrichment in the GluN2B/PSD-95 condensates under the "Basal" condition (Fig. 5c). After stimulation

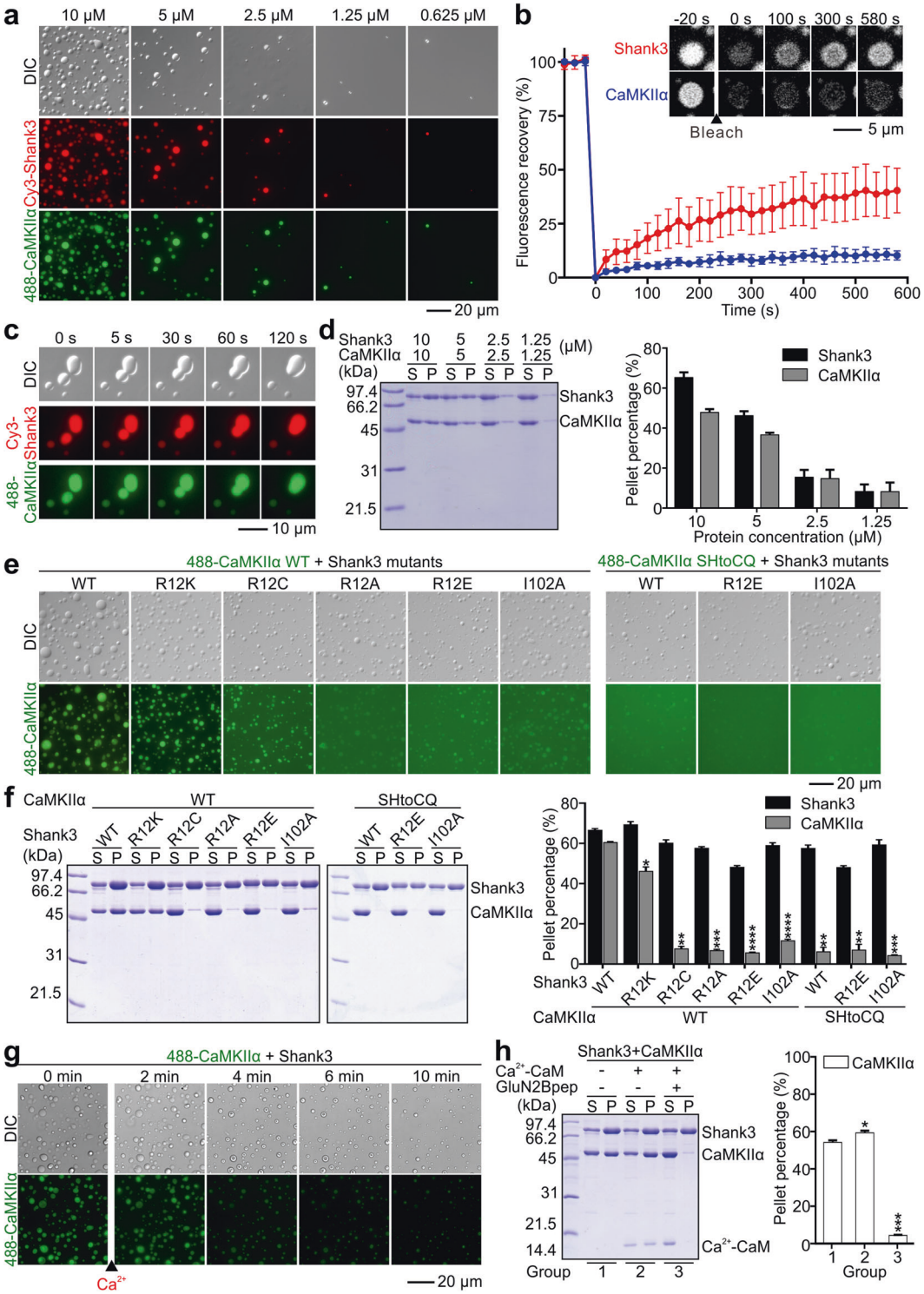

by $CaCl_2$, CaMKIIα was dramatically enriched into condensed droplets, accompanied by increased phase separation of both PSD-95 and GluN2B (Fig. 5c, e; Supplementary information, Movie S2). Addition of EGTA to the Ca^{2+}-stimulated CaM/CaMKIIα/GluN2B/PSD-95/PP2A mixture led to time-dependent dispersion of the CaMKIIα/GluN2B/PSD-95 condensates, and the system returned to the basal-like condition (Fig. 5c, e; Supplementary information, Movie S3). The sedimentation-based LLPS assay provided a semi-quantitative assay showing the Ca^{2+}-dependent reversible CaMKIIα/GluN2B/PSD-95 formation as in the imaging-based study (Fig. 5d). The sedimentation-based assay also showed that CaMKIIα were phosphorylated under the stimulated condition as indicated by the upward shifting of the bands (Fig. 5d). Removal of Ca^{2+} led to quantitative dephosphorylation of CaMKIIα by PP2A (Fig. 5d). Thus, we conclude that CaMKIIα is not enriched in the GluN2B/PSD-95 condensates at the basal condition; the rise of Ca^{2+} concentration activates CaMKIIα and promotes the enzyme to enter the GluN2B/PSD-95 condensates. The activated enzyme in return also enhances phase separation of PSD-95 and GluN2B. Removal of Ca^{2+} leads to

Fig. 4 CaMKIIα can be enriched into Shank3 condensates through direct interaction. a DIC and fluorescence images showing Shank3 and CaMKIIα underwent LLPS at indicated concentrations. The NaCl concentration of the buffer was 150 mM. Only 1% of each protein was sparsely labeled by the indicated fluorophores. The NaCl concentration and the fluorophore labeling ratio was used throughout this study unless otherwise specified. **b** FRAP experiments showing the recovery curves of the fluorescence signals in the condensed phase of Shank3 and CaMKIIα after photobleaching. The concentrations of both Shank3 and CaMKIIα were 10 μM. Only the protein to be analyzed was Cy3-labeled. The curves represent the averaged signals from 5 droplets with a diameter of ~4 μm. All data are presented as means ± SD. **c** DIC and fluorescence images showing the condensed droplets formed by Shank3 and CaMKIIα fused together to generate larger droplets over time. The concentrations of Shank3 and CaMKIIα were 10 μM. **d** Representative SDS-PAGE analysis and quantification data showing the distributions of Shank3 and CaMKIIα in the supernatant (S) and pellet (P) in the sedimentation-based assays with the indicated protein concentrations. **e** DIC and fluorescence images showing mutations of Shank3 or CaMKIIα weakened or abolished the enrichment of CaMKIIα into the Shank3 condensates. 10 μM unlabeled Shank3 was mixed with 10 μM iFluor 488-labeled CaMKIIα. **f** Representative SDS-PAGE analysis and quantification data showing the distributions of Shank3 and CaMKIIα in the supernatant (S) and pellet (P) in the sedimentation-based assays. The concentrations of both Shank3 and CaMKIIα were 10 μM. **g** DIC and fluorescence images showing that, in the presence of GluN2Bpep, the CaMKIIα/Shank3 droplets were gradually dispersed by Ca^{2+}-CaM. The concentration of Shank3 and CaMKIIα was 5 μM. The final concentration of GluN2Bpep and CaM was 50 μM. **h** Representative SDS-PAGE analysis and quantification data showing that Ca^{2+}-CaM can disperse CaMKIIα from the Shank3 condensates. The concentration of each component was 10 μM. Statistical data in **d**, **f**, and **h** are presented as means ± SD, with results from 3 independent batches of sedimentation experiments. $^{*}P < 0.05$; $^{**}P < 0.01$; $^{***}P < 0.001$; $^{****}P < 0.0001$ using one-way ANOVA with Dunnett's multiple comparisons test.

dephosphorylation of CaMKIIα by PP2A (and possibly by PP1 as well in synapses), conversion of CaMKIIα back to autoinhibited conformation, and concomitant dispersion of the CaMKIIα/GluN2B/PSD-95 condensates. The above data provide a biochemical foundation showing that CaMKIIα can shuttling between two distinct PSD subcompartments or nano-domains in responding Ca^{2+} concentration oscillations, a phenomena that has been captured by EM in real synapses in situ.[5,6]

Activation of CaMKIIα further promotes PSD assembly via phosphorylating SAPAP

NMDAR activation-mediated Ca^{2+} influx is expected to activate CaMKIIα in the lower layer of PSD or even the enzyme in spine cytoplasm and dendritic shaft. To investigate the possible role of the CaMKIIα activation on the PSD assembly regulation, we first investigated whether CaMKIIα could co-phase separate with the reconstituted PSD condensates containing four major scaffold proteins (PSD-95, SAPAP, Shank3, and Homer3, termed 4×PSD; Fig. 6a).[13] DIC and fluorescence imaging studies indicated that CaMKIIα was enriched into and perfectly co-localized with other proteins in the condensed droplets formed by the 4×PSD assembly (Fig. 6b). Sedimentation-based assay showed that co-phase separation with PSD led to massive enrichment of CaMKIIα into the PSD condensates (Supplementary information, Fig. S5a). The recruitment of CaMKIIα to the PSD condensates also required the specific interaction between CaMKIIα and Shank3 NTD-ANK, as each of the mutation disrupted the CaMKIIα/Shank3 interaction also impaired CaMKIIα's recruitment to the PSD condensates (Supplementary information, Fig. S5a).

We next tested how an activated CaMKIIα might modulate PSD phase separation. In all experiments containing ATP, we used 0.5 mM of ATP, which is much higher than the concentrations of CaMKIIα and the rest of the components in the mixtures (typically at 10 μM or below) and we demonstrated that 0.5 mM ATP barely impacted the phase separation of the Shank3 and CaMKIIα mixture as a hydrotrope (Supplementary information, Fig. S5b).[41] Interestingly, addition of Ca^{2+} to the reconstituted 4×PSD with apo-CaM and CaMKIIα led to increases of both signal intensity and droplet area of the PSD assemblies (Fig. 6c, d; Supplementary information, Movie S4), an observation reminiscent of synaptic activity-induced structural LTP.

What might be the molecular mechanism underlying Ca^{2+}-induced PSD assembly enlargement? SAPAPs are known to be phosphorylated by CaMKII in vitro and in cultured neurons.[42–44] Importantly, phosphorylation of the specific sites in PSD-95 binding repeats (S352, S381 and S412) can increase the binding affinity of SAPAP to PSD-95 by more than 1000-fold.[45] We next investigated the impact of CaMKIIα-mediated SAPAP phosphorylation on the PSD condensate formation by imaging. We compared time-dependent PSD-95 enrichments into PSD condensates after CaMKIIα activation. Since phase separation by itself is a time-dependent process, we included the SAPAP-"AAA" (S352A, S381A and S412A) as the control. This fluorescence imaging experiments clearly showed that PSD-95 showed a time-dependent incorporation into the PSD condensate upon CaMKIIα activation. In contrast, the level of PSD-95 change and the size of the droplets in the SAPAP-"AAA" control group was minimal (Fig. 6e, f; Supplementary information, Movie S5).

Further sedimentation-based assays demonstrated that activation of CaMKIIα led to a dramatic increase of PSD-95 enrichment into the PSD condensates (Fig. 6g; note that the mobility of SAPAP is obviously up-shifted upon phosphorylation by the activated enzyme). As the control, the kinase dead mutant of CaMKIIα (D135N, labeled as "DN" in Fig. 6g) had no impact on the LLPS of PSD-95 and other proteins. Importantly, in the SAPAP-"AAA" control group, activation of CaMKIIα had no impact on the PSD-95 recruitment to the PSD condensates (Fig. 6g). It should be noted that we used PSD-95 as the read-out for the enhanced PSD assembly, a process caused by strengthened interaction between PSD-95 and phosphorylated SAPAP. Since PSD-95 is stably associated with the PSD membranes, CaMKIIα-mediated phosphorylation of SAPAP would strengthen the lower layer of PSD components (e.g., Shank/Homer) with the upper layer PSD components (e.g., glutamate receptor/PSD-95/SAPAP),[13] instead of PSD-95 movements in our in vitro assay. Such CaMKIIα activity-dependent enhancement of PSD condensate formation is analogous to the structural enlargements of synapses and PSDs upon stimulation, a term frequently referred to as structural LTP in the field.[7–9]

DISCUSSION

CaMKIIα can decode the frequency and amplitude of synaptic Ca^{2+} transients, via its multiple conformations.[1,27,46–55] Owing to its extremely high abundance in synapse and the dodecameric architecture, CaMKII decodes and transduces synaptic Ca^{2+} signals both as a kinase and as a scaffold. The fact that the concentration of CaMKIIα in synapse is higher than most of its substrates suggests that each enzyme molecule may only need to perform one cycle of catalytic reaction upon each synaptic stimulation pulse. As such, CaMKIIα is a very unusual enzyme/scaffold.[1–4] Accordingly, it is extremely difficult to assign a particular synaptic function to a specific conformational state or an action mechanism of CaMKIIα, which is often elucidated from in vitro studies. We show in this study that the reconstituted PSD condensates can function as a valuable platform to bridge in vitro studies of

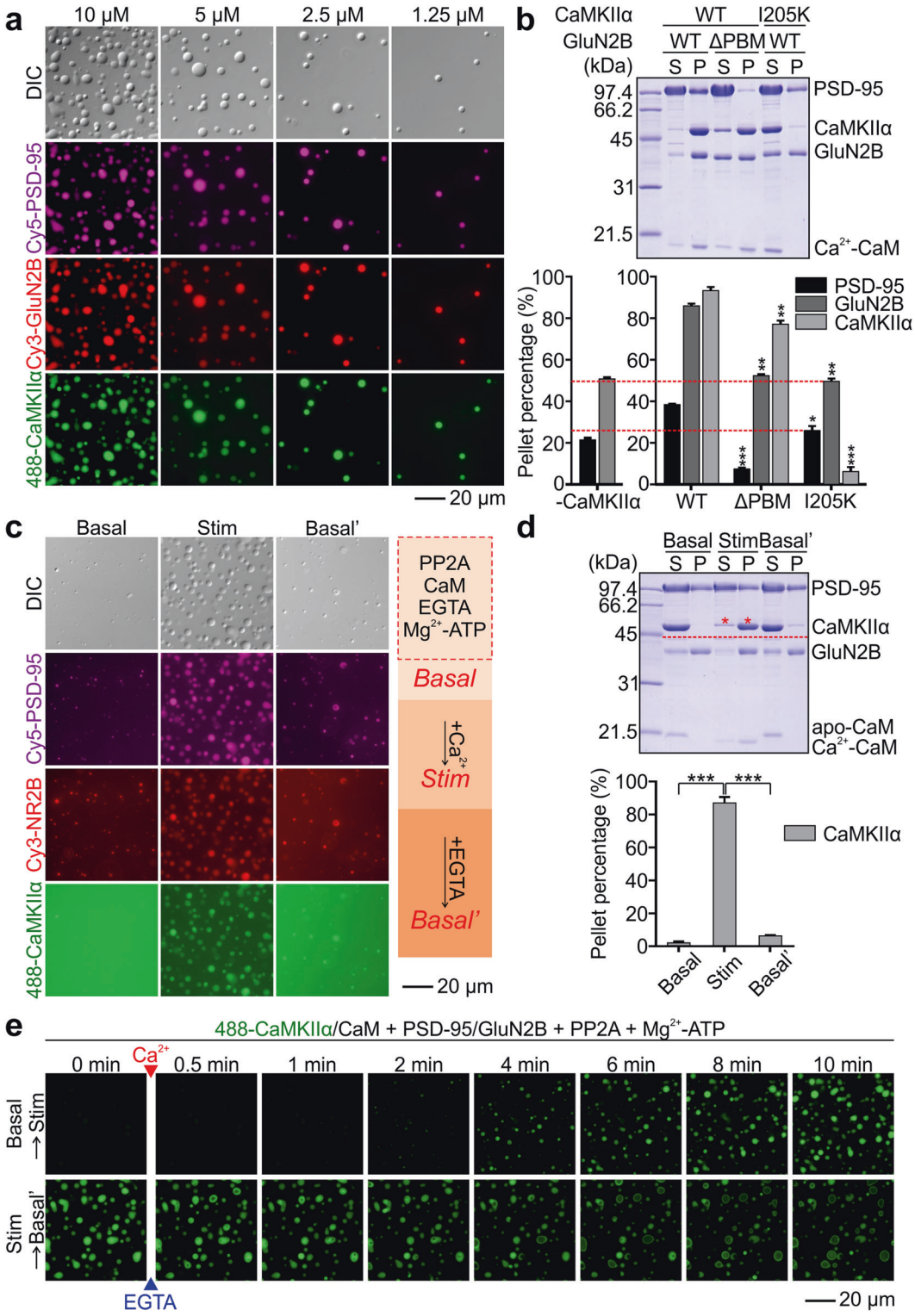

CaMKIIα and the functions of the enzyme in synapses. We demonstrated that, in the presence of CaMKIIα, the PSD condensates can reversibly respond to stimulations (e.g., Ca^{2+} concentration oscillation) and display activity-dependent structural enlargement/shrinkage cycle (Fig. 5), an observation reminiscent of synaptic structural plasticity. It is likely that this in vitro system, when combined with biochemical studies and functional experiments in vivo, may offer valuable insights into the molecular mechanisms governing synaptic plasticity and learning. The system may also hold potential in understanding why alterations of protein components in the PSD assemblies can lead to synaptic malfunctions and thus manifest into various brain diseases.

Several PSD proteins are reported to associate with CaMKIIα, and almost all of them interact with the activated enzyme.[23,32,56,57] The interaction between CaMKIIα and GluN2B

Fig. 5 GluN2B recruits activated CaMKIIα into GluB2B/PSD-95 condensates. a DIC and fluorescence images showing PSD-95, GluN2B and CaMKIIα underwent LLPS at the indicated concentrations. **b** Representative SDS-PAGE analysis and quantification data showing the distributions of PSD-95, GluN2B and CaMKIIα in the supernatant (S) and pellet (P) in the sedimentation-based assays. Various mutations of GluN2B or CaMKIIα were also analyzed. The concentration of each component was 10 μM. The quantification data of GluN2B/PSD-95 condensates (10 μM) from Supplementary information, Fig. S4d were adapted as a control for the comparison with the I205K group (red dashed lines). **c-d** DIC and fluorescence images (**c**) and sedimentation-based assays (**d**) showing Ca^{2+} and phosphatase-dependent, reversible CaMKIIα enrichment in the GluB2B/PSD-95 condensates. The "Basal" condition contained 0.5 mM ATP, 10 mM $MgCl_2$ and 2 mM EGTA. The "Stim" (i.e. stimulated) condition contained 0.5 mM ATP, 10 mM $MgCl_2$ and 2 mM $CaCl_2$. The "Basal" condition was based on the stimulated condition, then 4 mM EGTA was added after phosphorylation reaction was lasted for 2 min. The concentration of each component was 10 μM, except PP2A was at 0.5 μM. The NaCl concentration in the assay buffers was 100 mM. The red asterisks indicate the phosphorylated CaMKIIα. **e** Fluorescence images showing the gradual enrichment of CaMKIIα into GluN2B/PSD-95 condensates by adding $CaCl_2$ to the basal condition (upper panel) and gradual dispersions of CaMKIIα from GluN2B/PSD-95 condensates by adding EGTA to the stimulated condition (lower panel). The concentration of each component was 5 μM, except PP2A was at 0.5 μM. The NaCl concentration in the assay buffers was 100 mM. Statistical data in **b** and **d** are presented as means ± SD, with results from three independent batches of sedimentation experiments. *$P < 0.05$; **$P < 0.01$; ***$P < 0.001$ using one-way ANOVA with Dunnett's multiple comparisons test.

is particularly important, as this interaction is essential for the basal AMPAR synaptic transmission and NMDAR-dependent LTP.[3,4,52] In this study, we identified Shank3 as a specific binding partner of CaMKIIα in PSD. The N-terminal NTD-ANK tandem of Shank3 specifically and robustly binds to the autoinhibited CaMKIIα. Given that Shank3 is highly abundance in PSDs, one might envision that Shank3 may function to retain the autoinhibited form of CaMKIIα within PSD and poise the enzyme for next cycle of stimulation, a mechanism suitable for responding to high frequency synaptic stimulations. Recently, Perfitt et al. reported that the activated CaMKIIα can bind to Shank3 via a small fragment between the PDZ domain and the Homer binding sequence of Shank3.[23] The site is not included in this study of Shank3. Considering the abundance of CaMKIIα in PSD, it is possible that the full-length Shank3 may also be able to enrich activated CaMKIIα through the site after stimulation and facilitate phosphorylation of PSD proteins including SAPAPs and Shank3.[58] In real synapse, CaMKII are hetero-dodecamers primarily composed of α and β isozymes. Since actin filaments are not known to penetrate into the condensed PSDs and the concentrations of CaMKIIα within PSDs is known to be considerably higher than CaMKIIβ,[3,4] the molecular events elucidated for CaMKIIα in this study should apply to CaMKII hetero-dodecamers in synapses.

Immunogold EM studies in situ have revealed that Shank3 is located in the lower layer of PSD (aka PSD "pallium") together with Homer, whereas GluN2B together with PSD-95 is in the upper layer of the PSD immediately below the synaptic membranes (aka "PSD core").[6,22] Upon stimulation, a portion of CaMKIIα moves closer to the postsynaptic membrane, accompanied by a prominent enlargement of the lower layer of PSD assembly. Our in vitro reconstituted PSD condensates containing CaMKIIα recapitulate the EM-derived observations in situ. It is noted that no available technology can monitor such Ca^{2+}-dependent shuttling between distinct subcompartments within a distance of a few tens of nanometers in living synapses. Therefore, our in vitro reconstitution experiments provide a biochemical foundation for distinct PSD nano-domain formation as well as dynamic communications between subcompartments. Additionally, our findings also offer molecular mechanisms underlying the activity-induced PSD structural changes (Fig. 7). The entry of Ca^{2+} via NMDAR upon stimulation activates a portion of CaMKIIα, and the activated CaMKIIα can be efficiently clustered to the GluN2B/PSD-95 condensates in the "PSD core" (Fig. 5c, d). The active CaMKIIα can then phosphorylate SAPAP (and likely other proteins as well), which leads to a massive binding enhancement between SAPAP and PSD-95 and subsequent enlargement of the PSD assembly (Fig. 6). Protein phosphatases (PP2A and PP1) in PSD function as gatekeepers to terminate synaptic Ca^{2+} signal by dephosphorylating proteins phosphorylated by CaMKIIα including the enzyme itself. The binding between Shank3 and CaMKIIα may ensure that the inactivated enzyme do not all diffuse away from PSD, thus creating a pool of CaMKIIα to be able to rapidly response to next cycles of stimulations. Therefore, balanced actions of CaMKIIα and phosphatases within the PSD subcompartments provide a foundation to interpret frequencies and amplitudes of synaptic Ca^{2+} signals (Fig. 7). For example, if a stimulation paradigm leads to a net higher CaMKIIα activity over the phosphatase activities, the synapse is strengthened. Conversely, if stimulations of a synapse can not sustain net CaMKIIα-mediated substrate phosphorylation (i.e., the actions of phosphatases overtake those of CaMKIIα under weak stimulation conditions), the synapse gets weakened. Certainly, such simplistic model ought to be tested by experiments in the future.

MATERIALS AND METHODS

Constructs and peptide

Rat CaMKIIα (Uniprot: P11275) and mouse CaMKIIβ (Uniprot: P28652) were PCR-amplified from rat and mouse brain cDNA library. Various fragments and chimeric constructs of CaMKII were generated by the standard PCR method and individually inserted into a pEGFP-C3 vector with N-terminal EGFP tag for expression in HEK293T cells or a pET vector with a N-terminal His_6-SUMO tag for expression in *Escherichia coli*. The NTD-ANK fragment of Shank3 (Genbank: AB231013) has the same amino acid boundaries as previously reported,[37] and was inserted into the pGEX-4T-1 vector (GE Healthcare) with N-terminal GST tag for affinity purification and the GST pull-down experiments. The simplified version of Shank3 was generated by using an overlap PCR method to fuse multiple fragments, including residues 1–376 (NTD-ANK), 533–665 (N-PDZ), 1294–1323 (HBS), 1400–1426 (CBS) and 1654–1730 (SAM) with three point mutations (L231R, F304Y and M1718A) to improve solubility and homogeneity of the recombinant protein. The gene was inserted into a modified version of pET-32a with an N-terminal GB1-His_6 tag and an HRV-3C cutting site following the GB1-His_6 tag. The cytoplasmic tail of GluN2B (Uniprot: Q00960; aa 1170–1482) was cloned into a modified version of pET-32a with an N-terminal GB1-His_6 tag and an HRV-3C cutting site. All other constructs of PSD components are the same as previously reported.[13] Human PP1γ catalytic subunit (Uniprot: P36873) was from Addgene (plasmid #44225).[59] PP1γ was cloned into a modified version of pET-32a with an N-terminal GB1-His_6 tag and an HRV-3C cutting site. Mouse PP2A catalytic subunit (Uniprot: P63330) was amplified from a mouse brain cDNA library and inserted into pFastbac1 vector with an N-terminal TwinStrepII-His_8 tag for Bac-to-Bac baculovirus expression system (Thermo Fisher). All mutants were generated by the standard PCR-based method. All constructs were confirmed by DNA sequencing.

The GluN2Bpep peptide (sequence: KAQKKNRNKLRRQH-SYDTFVDL) was commercially synthesized by ChinaPeptides (Shanghai, China) with purity > 99%.

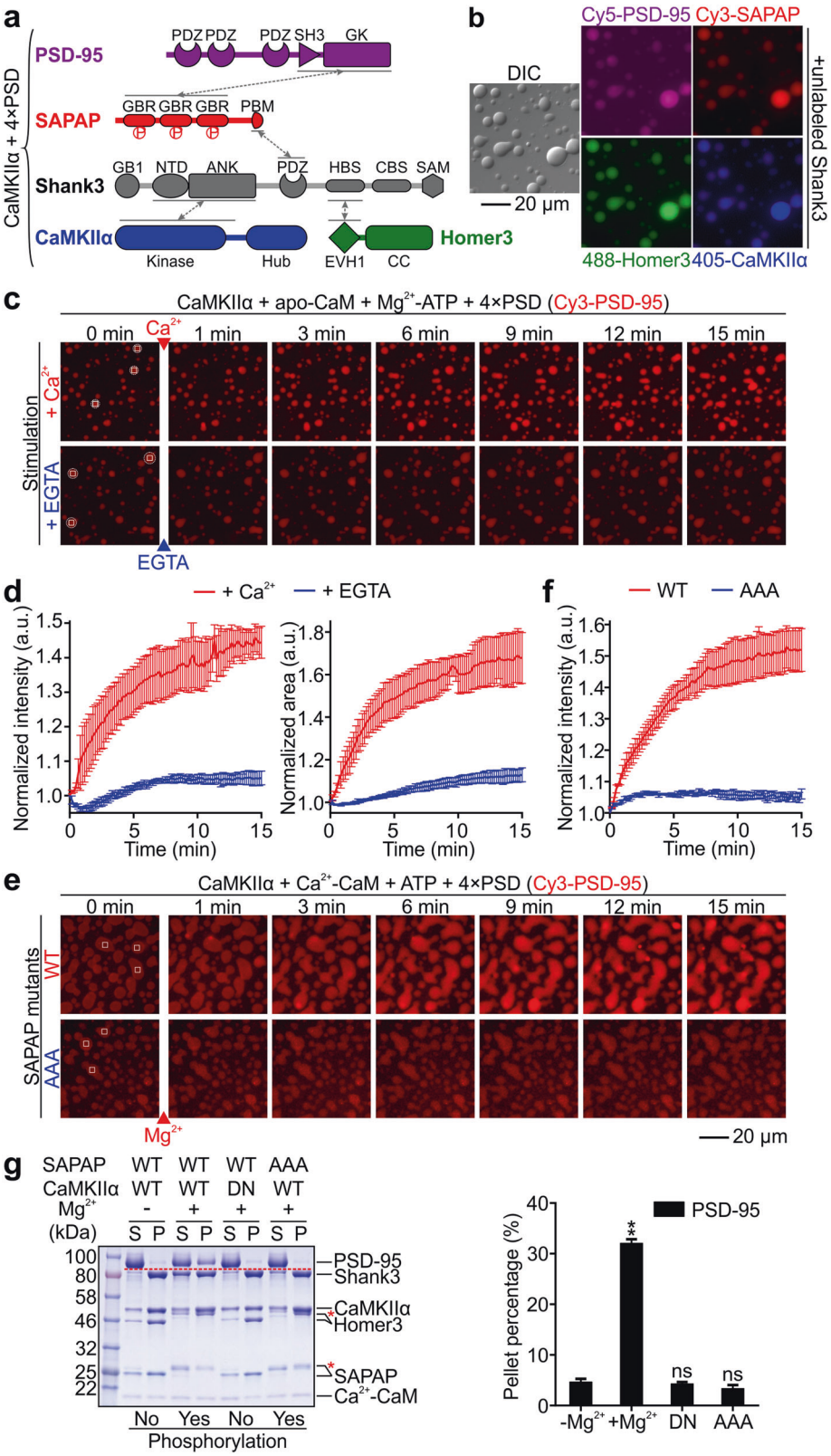

Protein expression and purification

The WT and variants of CaMKIIα holoenzyme was expressed and purified according to the previous reported protocol.[27] Briefly, His_6-SUMO tagged CaMKIIα was co-expressed with λ phosphatase in *Escherichia coli* BL21-CodonPlus(DE3)-RIL cells (Agilent Technologies) in LB medium at 16 °C. Recombinant CaMKIIα was purified by Ni^{2+}-NTA (GE Healthcare) affinity chromatography followed by Superdex 200 26/600 size-exclusion chromatography. After Ulp1 protease treatment at 4 °C overnight to cleave the SUMO tag, the sample was loaded onto a Mono Q column, and

Fig. 6 CaMKIIα phosphorylates SAPAP and enhances PSD condensate formation. a Schematic diagram showing the protein-protein interaction network of 4×PSD and CaMKIIα. **b** DIC and fluorescence images showing CaMKIIα and 4×PSD undergo LLPS. PSD-95, SAPAP, Homer3 and CaMKIIα were labeled by different fluorophores as indicated and were co-localized in condensed droplets. Shank3 was not labeled and thus invisible. The concentration of each component was 10 μM. **c** Fluorescence images showing the gradual enrichment of PSD-95 into CaMKIIα-containing PSD condensates by addition of Ca^{2+} (but not by EGTA). The concentration of each component was 2 μM. **d** Time-dependent, CaMKIIα phosphorylation-induced Cy3-PSD-95 signal intensity increase (left panel) and droplet area increase of the PSD condensates (right panel) with addition of Ca^{2+} or EGTA in **c**. The curves of normalized fluorescence intensities represent the averaged signals from 3 regions with a side length of ~3.25 μm indicated as white squares in **c**. The curves of normalized areas represent the areas of 3 droplets with dashed circles in **c**. All data are presented as means ± SD. **e** Fluorescence images showing the gradual enrichment of PSD-95 into CaMKIIα-containing PSD condensates by addition of $MgCl_2$ to initiate the phosphorylation reaction. The "AAA" mutant of SAPAP1, which does not have the specific CaMKIIα-phosphorylation sites and thus could not enhance PSD-95 recruitment to PSD condensates. The concentration of each component was 2 μM. **f** Time-dependent, CaMKIIα phosphorylation-induced Cy3-PSD-95 signal increase in the PSD condensates containing the WT SAPAP1 (WT) or the "AAA" mutant (AAA). The curves represent the averaged signals from 3 regions with a side length of ~3.25 μm indicated as white squares in **e**. All data are presented as means ± SD. **g** Representative SDS-PAGE analysis and quantification data showing CaMKIIα can phosphorylate SAPAP1 at specific sites to enhance the PSD-95 enrichment in the condensed PSD phase. The concentration of each component was 10 μM. The red asterisks indicate the phosphorylated Homer3 and SAPAP. The results are presented as means ± SD from 3 independent batches of sedimentation experiments. ns, not significant; $^{**}P < 0.01$ using one-way ANOVA with Dunnett's multiple comparisons test.

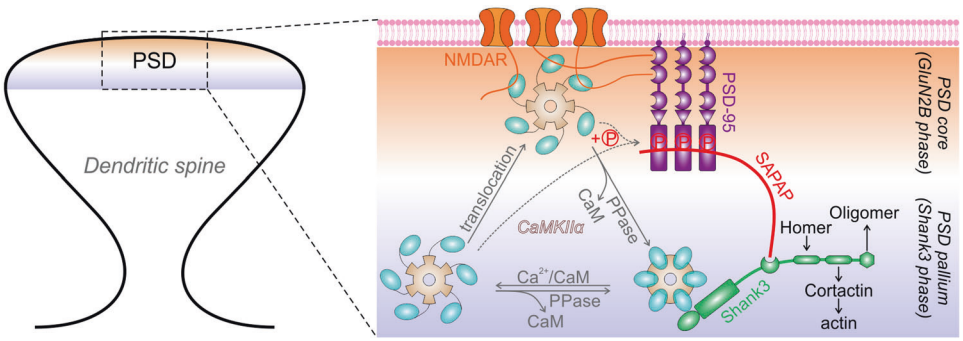

Fig. 7 A model depicting Ca^{2+}-dependent, phosphatase-regulated CaMKIIα activity cycling in different layers of PSD. The CaMKIIα activity cycle also reversibly modulates PSD assembly formation and dispersion.

eluted by a NaCl gradient. The eluted protein was then loaded onto a Superose 6 10/300 gel filtration column for the final step purification. All buffers used for CaMKIIα purification contained 10% glycerol. The final buffer was 50 mM Tris, pH 8.0, 200 mM NaCl, 10% glycerol, 5 mM DTT. The purified CaMKIIα was concentrated to 80 μM and stored at −80 °C.

PP2A was expressed by Bac-to-Bac baculovirus expression system. The recombinant virus was obtained by transposition, transfection, and serial steps of amplification using *sf9* cells (Thermo Fisher) according to the manufacturer's instructions. For expression, 4 L of High Five cells (Thermo Fisher) with the density ~2.0×10^6 cells per mL were infected by baculovirus and incubated at 19 °C for 120 h.[60] Recombinant PP2A was firstly purified using Strep-Tactin XT Superflow resin (IBA) and then loaded onto a Superose 12 10/300 gel filtration column for final step purification with the buffer containing 50 mM, Tris pH 8.0, 100 mM NaCl, 2 mM DTT. The purified PP2A was concentrated to 50 μM and stored at −80 °C.

All other proteins were expressed in *Escherichia coli* BL21-CodonPlus(DE3)-RIL cells (Agilent Technologies) in LB medium at 16 °C. Recombinant proteins were firstly purified using Ni^{2+}-NTA Sepharose resin (GE Healthcare) for His_6-tagged proteins or GSH Sepharose resin for GST-tagged proteins (GE Healthcare). The Superdex 200 26/600 or Superdex 75 26/600 gel filtration columns were used for further purification. The affinity tag of each protein, except for Shank3 and the GST-tagged proteins, was cleaved by HRV-3C protease at 4 °C overnight and removed by another step of gel filtration chromatography. The final buffer of Shank3 was 50 mM Tris, pH 8.0, 500 mM NaCl, 2 mM DTT. For the other proteins, the final buffer was 50 mM Tris, pH 8.0, 100 mM NaCl, 2 mM DTT. All proteins were concentrated, aliquoted and stored at −80 °C for further experiments.

Affinity-purification coupled to mass spectrometry (AP-MS)

Two rat brains were dissected and lysed using Potter-Elvehjem style tissue homogenizer on ice in the lysis buffer containing 50 mM HEPES, pH 7.2, 0.6 M NaCl, 15% Glycerol, 20 mM CHAPS, 0.1% Triton X-100, 1 mM DTT, 1 mM EDTA, 1 mM EGTA and a cocktail of protease inhibitors (Merck). After ultracentrifugation (100,000× *g* for 30 min), the lysate was dialyzed against a buffer containing 20 mM HEPES, pH 7.2, 0.1 M NaCl, 5% Glycerol, 1 mM DTT, 1 mM EDTA, 1 mM EGTA. Fresh DTT and protease inhibitors was added before another step of ultracentrifugation (100,000× *g* for 2 h). The supernatant of rat brain lysate with protein concentration ~10 mg/mL was taken as prey for affinity purification.

For affinity purification, 2 nmol purified recombinant GST, GST-Shank3-SH3-PDZ and GST-Shank3-NTD-ANK were individually coupled to fresh GSH Sepharose resin. 1 mL of rat brain lysate was mixed with the bait-charged GSH Sepharose resin at 4 °C for 2 h. After extensive washing with the dialysis buffer with 0.1 % Triton X-100, the captured proteins were eluted by the elution buffer containing 20 mM HEPES, pH 8.0, 9 M Urea. In-solution trypsin digestion was carried out using Trypsin Gold (Promega) according to the manufacturer's instructions. The digested peptides were subjected to StageTip C18[61] desalting and MS analysis. Peptides were resuspended in 0.1% (v/v) formic acid and analyzed with a Q-Exactive Orbitrap mass spectrometer (Thermo Fisher) or Orbitrap Fusion mass spectrometer (Thermo Fisher).

GST pull-down assay

For GST pull-down assays using HEK293T cells expressing CaMKII, HEK293T cells were transiently transfected with various GFP-CaMKII encoding plasmids using Lipofectamine and Plus reagents (Thermo Fisher). Cells were harvested at 20 h post-transfection and lysed using the lysis buffer containing 50 mM Tris, pH 7.5, 150

mM NaCl, 1% Triton X-100 and a cocktail of protease inhibitors (Merck). For GST pull-down assay using purified CaMKII, the purified CaMKII was diluted into TBS buffer to the final concentration of 1 μM for the following steps.

For the GST pull-down assays detected by Coomassie Brilliant Blue staining (CBB, for Fig. 3d), 2 nmol purified CaMKIIα was mixed in 1 mL TBS (50 mM Tris, pH 7.5, 150 mM NaCl) with various conditions (Fig. 3b). For the GST pull-down assays detected by western blot, 0.1 mL cell lysate or diluted CaMKII (1 μM) were mixed with 0.9 mL TBS with various conditions (Fig. 3b). After autophosphorylation at room temperature for 5 min when needed, 2 nmol of purified GST-fused protein was added. The mixture was incubated at 4 °C for 30 min. After centrifugation at 16,873× *g* for 5 min, the supernatant was mixed with 40 μL of fresh GSH Sepharose resin and incubated for another 30 min. After extensive washing with corresponding wash buffer (Fig. 3b, TBS with 5 mM DTT and 1 mM EGTA or 1 mM $CaCl_2$), the captured proteins were eluted by SDS-PAGE loading buffer with boiling, resolved by SDS-PAGE, and immunoblotted with specific antibodies. Protein signals were visualized by an HRP-conjugated secondary antibody (Thermo Fisher) and Luminata Forte western HRP substrate (Merck).

Acetone precipitation

The GST pull-down assay system was scale down to 0.3 mL with concentrations of all components were the same as in the 1 mL system. After autophosphorylation at room temperature for 5 min, the mixture was incubated on ice for 1 h without addition of the respective GST-fused proteins to mimic the incubation during GST pull-down assay. Then 1.2 mL cold acetone was added to each mixture before incubation at −20 °C for 1 h. After centrifugation at 16,873× *g* for 10 min at 4 °C, the pellet was air-dried for 10 min at room temperature. Then the pellet was resuspended in 20 μL SDS-PAGE loading buffer. The samples were resolved by SDS-PAGE and immunoblotted with specific antibodies. Protein signals were visualized by an HRP-conjugated secondary antibody (Thermo Fisher) and Luminata Forte western HRP substrate (Merck).

Protein labeling with chemical fluorophore

The chemical fluorophores, including iFluor 488/Cy3/Cy5 NHS esters (AAT Bioquest), were dissolved in DMSO with the concentration of 10 mg/mL. The buffer of each purified proteins was exchanged using a HiTrap desalting column (GE Healthcare) to replace 50 mM Tris by 100 mM $NaHCO_3$, pH 8.3 with the rest of buffer condition unchanged. The fluorophores were added to protein solution with 1:1 molar ratio and incubated at room temperature for 1 h. After quenched by 0.2 M Tris, pH 8.0, labeled protein was exchanged into the original storage buffer using a HiTrap desalting column. Fluorescence labeling efficiency was detected using Nanodrop 2000 (Thermo Fisher).

LLPS assays

In vitro LLPS assays were carried out according to the previous reported protocol.[12,13] Briefly, all purified proteins were pre-cleared through high speed centrifugation (16,873× *g* for 10 min) at 4 °C in their storage buffer prior to LLPS assays. Proteins were directly mixed to reach specified protein concentrations. The NaCl concentration in the buffers for LLPS assay was carefully adjusted to reach specified concentration. Fresh DTT was added to the final concentration of 2 mM to avoid potential protein aggregation. To avoid potential impact of the hydrophobic dyes on phase separation assays, only 1% of each protein was dye-labeled by mixing labeled and unlabeled protein at the 1:99 ratio.

For sedimentation-based assays, the total volume of each mixture was 50 μL. After incubation at room temperature for 10 min, the mixture was centrifuged at 16,873× *g* at 22 °C for 5 min. The supernatant was collected, and the pellet was washed with 50 μL of the same buffer and thoroughly resuspended with 50 μL buffer. Samples from supernatant fraction and pellet fraction were analyzed by SDS-PAGE with Coomassie blue R250 staining. Three repeats were performed for each group. The intensity of each band on SDS-PAGE was quantified by ImageJ and data were presented as means ± SD.

For microscope-based assay, the total volume of each mixture is 20 μL. Each mixture was injected into a home-made chamber composed of a coverslip and a glass slide assembled with one layer of double-sided tape. DIC images and fluorescent images were captured at room temperature using a Nikon Ni-U upright fluorescence microscope with a 60× 1.40 N.A. oil objective lens.

For live imaging of the formation/dispersion of condensed droplets, the total volume of each mixture is 50 μL. The mixture was injected into a well of a 96-well glass-bottomed plate (Thermo Fisher). DIC images and fluorescent images were captured at room temperature using a Nikon Eclipse Ti-2 fluorescence microscope base equipped with an andor iXon Life EMCCD camera (Oxford Instruments) with a 100× 1.49 N.A. oil objective lens.

FRAP assay

FRAP experiments were carried out at room temperature on a Zeiss LSM 880 confocal microscope with a 63× 1.4 N.A. oil objective. Specifically, 2× zoom-in and a square region of interest (ROI) with the side length of 30 pixels (~4 μm, for the whole droplet) or 15 pixels (~2 μm, for the ROI inside the droplet) was performed for FRAP. In each FRAP experiment, fluorescence intensities of a neighboring droplet with similar size to the one used for photobleaching was recorded for fluorescence intensity correction and a third region in the background with the same size was also recorded for background signal subtraction. Cy3-labeled proteins were photobleached by 561 nm laser beams at 100% power. Each data point represented the averaged signal of five ROIs. All experiments were completed within 2 h after initiation of the phase separations. For data analysis, the intensity at the pre-bleach point was normalized to 100%, and the intensity right after the bleaching was set to 0%. Data were expressed as means ± SD.

ITC assay

ITC experiments were carried out using a VP-ITC calorimeter (Malvern) at 25 °C. All proteins used in ITC experiments were in the buffer containing 50 mM Tris, pH 8.0, 100 mM NaCl, 2 mM DTT and 1 mM $CaCl_2$. Each titration point was performed by injecting a 10 μL aliquot of one protein in the syringe into its binding protein in the cell at a time interval of 120 s to ensure that the titration peak returned to the baseline. Titration data were fitted with the one-site binding model using Origin 7.0 to derive the K_D values.

Protein docking

Docking of Shank3 NTD-ANK tandem to a subunit of CaMKIIα was performed using the software HADDOCK2.2[28] with one subunit of the crystal structures of CaMKII holoenzyme (PDB ID: 3SOA)[27] and Shank3 NTD-ANK tandem (PDB ID: 6KYK)[37] as the starting structures. The active residues used in the docking were chosen based on our GST pull-down data. Three residues (R12, I102 and D103) in Shank3 NTD-ANK and two residues (S272 and H273) in CaMKIIα were defined as active residues. All Shank3 NTD-ANK residues with relative solvent accessibility (RSA) greater than 30% were defined as passive residues, and the first 300 residues of CaMKIIα (including kinase domain and autoinhibitory segment) with RSA greater than 30% were also defined as passive residues. Then an ambiguous interaction restraint was defined with an upper distance of 2 Å. A total of 1000 rigid-body docking solutions were generated by energy minimizations. Then 200 structures with the best intermolecular energy scores were subjected to semi-flexible simulated annealing in torsion angle space followed by a final refinement in explicit water. The final structures were clustered using the interface ligand root-mean-square deviation

matrix and ranked according to their total intermolecular energy scores. All structure figures were produced using PyMOL (http://www.pymol.org/).

Quantification and statistical analysis

Statistical parameters including the definitions and exact values of n (e.g., number of experiments, number of droplets), distributions and deviations are reported in the figures and corresponding figure legends. Data were expressed as means ± SD. ns, not significant; *$P < 0.05$; **$P < 0.01$; ***$P < 0.001$; ****$P < 0.0001$ using one-way ANOVA with Dunnett's multiple comparisons test. Statistical analysis was performed in GraphPad Prism.

ACKNOWLEDGEMENTS

This work was supported by a grant from the Simons Foundation (Award ID: 510178), grants from RGC of Hong Kong (16101419, AoE-M09-12 and C6004-17G), and a grant from the Minister of Science and Technology of China (2019YFA0508402) to M.Z. M.Z. is a Kerry Holdings Professor of Science, a Croucher Foundation Senior Fellow and a Senior Fellow of IAS at HKUST.

AUTHOR CONTRIBUTIONS

Q.C., M. Zeng, X.W., H.W., Y.Z. performed experiments, Q.C., M. Zeng, X.W., H.W., Y.Z., R.T., M. Zhang analyzed data, Q.C., M. Zhang designed the research, Q.C., M. Zhang drafted and all authors commented on the paper, M. Zhang coordinated the project.

ADDITIONAL INFORMATION

Supplementary information accompanies this paper at https://doi.org/10.1038/s41422-020-00439-9.

Competing interests: The authors declare no competing interests.

REFERENCES

1. Lisman, J., Yasuda, R. & Raghavachari, S. Mechanisms of CaMKII action in long-term potentiation. *Nat. Rev. Neurosci.* **13**, 169–182 (2012).
2. Herring, B. E. & Nicoll, R. A. Long-term potentiation: from CaMKII to AMPA receptor trafficking. *Annu. Rev. Physiol.* **78**, 351–365 (2016).
3. Hell Johannes, W. CaMKII: claiming center stage in postsynaptic function and organization. *Neuron* **81**, 249–265 (2014).
4. Bayer, K. U. & Schulman, H. CaM kinase: still inspiring at 40. *Neuron* **103**, 380–394 (2019).
5. Zhu, J., Shang, Y. & Zhang, M. Mechanistic basis of MAGUK-organized complexes in synaptic development and signalling. *Nat. Rev. Neurosci.* **17**, 209–223 (2016).
6. Dosemeci, A., Weinberg, R. J., Reese, T. S. & Tao-Cheng, J. H. The postsynaptic density: there is more than meets the eye. *Front. Synaptic. Neurosci.* **8**, 23 (2016).
7. Lee, S. J., Escobedo-Lozoya, Y., Szatmari, E. M. & Yasuda, R. Activation of CaMKII in single dendritic spines during long-term potentiation. *Nature* **458**, 299–304 (2009).
8. Matsuzaki, M., Honkura, N., Ellis-Davies, G. C. & Kasai, H. Structural basis of long-term potentiation in single dendritic spines. *Nature* **429**, 761–766 (2004).
9. Bosch, M. et al. Structural and molecular remodeling of dendritic spine substructures during long-term potentiation. *Neuron* **82**, 444–459 (2014).
10. Takumi, Y., Ramirez-Leon, V., Laake, P., Rinvik, E. & Ottersen, O. P. Different modes of expression of AMPA and NMDA receptors in hippocampal synapses. *Nat. Neurosci.* **2**, 618–624 (1999).
11. Matsuzaki, M. et al. Dendritic spine geometry is critical for AMPA receptor expression in hippocampal CA1 pyramidal neurons. *Nat. Neurosci.* **4**, 1086–1092 (2001).
12. Zeng, M. et al. A binding site outside the canonical PDZ domain determines the specific interaction between Shank and SAPAP and their function. *Proc. Natl. Acad. Sci. USA* **113**, E3081–E3090 (2016).
13. Zeng, M. et al. Reconstituted postsynaptic density as a molecular platform for understanding synapse formation and plasticity. *Cell* **174**, 1172–1187 (2018).
14. Zeng, M. et al. Phase separation-mediated TARP/MAGUK complex condensation and AMPA receptor synaptic transmission. *Neuron* **104**, 529–543 (2019).
15. Chen, X., Wu, X., Wu, H. & Zhang, M. Phase separation at the synapse. *Nat. Neurosci.* **23**, 301–310 (2020).
16. Shen, K. & Meyer, T. Dynamic control of CaMKII translocation and localization in hippocampal neurons by NMDA receptor stimulation. *Science* **284**, 162–166. (1999).
17. Dosemeci, A. et al. Glutamate-induced transient modification of the postsynaptic density. *Proc. Natl. Acad. Sci. USA* **98**, 10428–10432 (2001).
18. Otmakhov, N. et al. Persistent accumulation of calcium/calmodulin-dependent protein kinase II in dendritic spines after induction of NMDA receptor-dependent chemical long-term potentiation. *J. Neurosci.* **24**, 9324–9331 (2004).
19. Biederer, T., Kaeser, P. S. & Blanpied, T. A. Transcellular nanoalignment of synaptic function. *Neuron* **96**, 680–696 (2017).
20. Tang, A. H. et al. A trans-synaptic nanocolumn aligns neurotransmitter release to receptors. *Nature* **536**, 210–214 (2016).
21. Choquet, D. Linking nanoscale dynamics of AMPA receptor organization to plasticity of excitatory synapses and learning. *J. Neurosci.* **38**, 9318–9329 (2018).
22. Tao-Cheng, J. H. Activity-dependent redistribution of CaMKII in the postsynaptic compartment of hippocampal neurons. *Mol. Brain* **13**, 53 (2020).
23. Perfitt, T. L. et al. Neuronal L-Type calcium channel signaling to the nucleus requires a novel CaMKIIalpha-Shank3 interaction. *J. Neurosci.* **40**, 2000–2014 (2020).
24. Moessner, R. et al. Contribution of SHANK3 mutations to autism spectrum disorder. *Am. J. Hum. Genet.* **81**, 1289–1297 (2007).
25. Gauthier, J. et al. Novel de novo SHANK3 mutation in autistic patients. *Am. J. Med. Genet. B Neuropsychiatr. Genet.* **150B**, 421–424 (2009).
26. Durand, C. M. et al. Mutations in the gene encoding the synaptic scaffolding protein SHANK3 are associated with autism spectrum disorders. *Nat. Genet.* **39**, 25–27 (2007).
27. Chao, L. H. et al. A mechanism for tunable autoinhibition in the structure of a human Ca2+/calmodulin- dependent kinase II holoenzyme. *Cell* **146**, 732–745 (2011).
28. Dominguez, C., Boelens, R. & Bonvin, A. M. HADDOCK: a protein-protein docking approach based on biochemical or biophysical information. *J. Am. Chem. Soc.* **125**, 1731–1737 (2003).
29. Myers, J. B. et al. The CaMKII holoenzyme structure in activation-competent conformations. *Nat. Commun.* **8**, 15742 (2017).
30. Rellos, P. et al. Structure of the CaMKIIdelta/calmodulin complex reveals the molecular mechanism of CaMKII kinase activation. *PLoS Biol.* **8**, e1000426 (2010).
31. Hoffman, L., Stein, R. A., Colbran, R. J. & McHaourab, H. S. Conformational changes underlying calcium/calmodulin-dependent protein kinase II activation. *EMBO J.* **30**, 1251–1262 (2011).
32. Bayer, K. U., De Koninck, P., Leonard, A. S., Hell, J. W. & Schulman, H. Interaction with the NMDA receptor locks CaMKII in an active conformation. *Nature* **411**, 801–805 (2001).
33. Patton, B. L., Miller, S. G. & Kennedy, M. B. Activation of type II calcium/calmodulin-dependent protein kinase by Ca2+/calmodulin is inhibited by autophosphorylation of threonine within the calmodulin-binding domain. *J. Biol. Chem.* **265**, 11204–11212 (1990).
34. Hashimoto, Y., Schworer, C. M., Colbran, R. J. & Soderling, T. R. Autophosphorylation of Ca2+/calmodulin-dependent protein kinase II. Effects on total and Ca2+-independent activities and kinetic parameters. *J. Biol. Chem.* **262**, 8051–8055 (1987).
35. Strack, S., Westphal, R. S., Colbran, R. J., Ebner, F. F. & Wadzinski, B. E. Protein serine/threonine phosphatase 1 and 2A associate with and dephosphorylate neurofilaments. *Brain Res. Mol. Brain Res.* **49**, 15–28 (1997).
36. Strack, S., Kini, S., Ebner, F. F., Wadzinski, B. E. & Colbran, R. J. Differential cellular and subcellular localization of protein phosphatase 1 isoforms in brain. *J. Comp. Neurol.* **413**, 373–384 (1999).
37. Cai, Q., Hosokawa, T., Zeng, M., Hayashi, Y. & Zhang, M. Shank3 binds to and stabilizes the active form of Rap1 and HRas GTPases via Its NTD-ANK tandem with distinct mechanisms. *Structure* **28**, 290–300 (2020). e294.
38. Frank, R. A. & Grant, S. G. Supramolecular organization of NMDA receptors and the postsynaptic density. *Curr. Opin. Neurobiol.* **45**, 139–147 (2017).
39. Long, J. F. et al. Supramodular structure and synergistic target binding of the N-terminal tandem PDZ domains of PSD-95. *J. Mol. Biol.* **327**, 203–214 (2003).
40. Kornau, H. C., Schenker, L. T., Kennedy, M. B. & Seeburg, P. H. Domain interaction between NMDA receptor subunits and the postsynaptic density protein PSD-95. *Science* **269**, 1737–1740 (1995).
41. Patel, A. et al. ATP as a biological hydrotrope. *Science* **356**, 753–756 (2017).
42. Collins, M. O. et al. Proteomic analysis of in vivo phosphorylated synaptic proteins. *J. Biol. Chem.* **280**, 5972–5982 (2005).
43. Shin, S. M. et al. GKAP orchestrates activity-dependent postsynaptic protein remodeling and homeostatic scaling. *Nat. Neurosci.* **15**, 1655–1666 (2012).
44. Trinidad, J. C., Thalhammer, A., Specht, C. G., Schoepfer, R. & Burlingame, A. L. Phosphorylation state of postsynaptic density proteins. *J. Neurochem.* **92**, 1306–1316 (2005).

45. Zhu, J. et al. Synaptic targeting and function of SAPAPs mediated by phosphorylation-dependent binding to PSD-95 MAGUKs. *Cell Rep.* **21**, 3781–3793 (2017).
46. Kennedy, M. B. Synaptic signaling in learning and memory. *Cold Spring Harb. Perspect. Biol*. **8**, a016824 (2013).
47. Lisman, J., Schulman, H. & Cline, H. The molecular basis of CaMKII function in synaptic and behavioural memory. *Nat. Rev. Neurosci.* **3**, 175–190 (2002).
48. Malenka, R. C. et al. An essential role for postsynaptic calmodulin and protein kinase activity in long-term potentiation. *Nature* **340**, 554–557 (1989).
49. Malinow, R., Schulman, H. & Tsien, R. W. Inhibition of postsynaptic PKC or CaMKII blocks induction but not expression of LTP. *Science* **245**, 862–866 (1989).
50. Silva, A. J., Stevens, C. F., Tonegawa, S. & Wang, Y. Deficient hippocampal long-term potentiation in alpha-calcium-calmodulin kinase II mutant mice. *Science* **257**, 201–206 (1992).
51. Chang, J. Y. et al. CaMKII autophosphorylation is necessary for optimal integration of Ca(2+) signals during LTP induction, but not maintenance. *Neuron* **94**, 800–808 (2017). e804.
52. Incontro, S. et al. The CaMKII/NMDA receptor complex controls hippocampal synaptic transmission by kinase-dependent and independent mechanisms. *Nat. Commun.* **9**, 2069 (2018).
53. Bhattacharyya M., Karandur D., Kuriyan J. Structural insights into the regulation of Ca(2+)/calmodulin-dependent protein kinase II (CaMKII). *Cold Spring Harb. Perspect. Biol.* **12**, a035147. https://doi.org/10.1101/cshperspect.a035147 (2020).
54. Chang, J. Y., Nakahata, Y., Hayano, Y. & Yasuda, R. Mechanisms of Ca(2+)/calmodulin-dependent kinase II activation in single dendritic spines. *Nat. Commun.* **10**, 2784 (2019).
55. Kim, K., Saneyoshi, T., Hosokawa, T., Okamoto, K. & Hayashi, Y. Interplay of enzymatic and structural functions of CaMKII in long-term potentiation. *J. Neurochem.* **139**, 959–972 (2016).
56. Saneyoshi, T. et al. Reciprocal activation within a kinase-effector complex underlying persistence of structural LTP. *Neuron* **102**, 1199–1210 (2019).
57. Baucum, A. J. 2nd, Shonesy, B. C., Rose, K. L. & Colbran, R. J. Quantitative proteomics analysis of CaMKII phosphorylation and the CaMKII interactome in the mouse forebrain. *ACS Chem. Neurosci.* **6**, 615–631 (2015).
58. Perfitt, T. L., Stauffer, P. E., Spiess, K. L. & Colbran, R. J. CaMKIIalpha phosphorylation of Shank3 modulates ABI1-Shank3 interaction. *Biochem. Biophys. Res. Commun.* **524**, 262–267 (2020).
59. Trinkle-Mulcahy, L., Sleeman, J. E. & Lamond, A. I. Dynamic targeting of protein phosphatase 1 within the nuclei of living mammalian cells. *J. Cell Sci.* **114**, 4219–4228 (2001).
60. Ikehara, T., Nakashima, S., Nakashima, J., Kinoshita, T. & Yasumoto, T. Efficient production of recombinant PP2A at a low temperature using a baculovirus expression system. *Biotechnol. Rep. (Amst)* **11**, 86–89 (2016).
61. Rappsilber, J., Mann, M. & Ishihama, Y. Protocol for micro-purification, enrichment, pre-fractionation and storage of peptides for proteomics using StageTips. *Nat. Protoc.* **2**, 1896–1906 (2007).
62. Erondu, N. E. & Kennedy, M. B. Regional distribution of type II Ca2+/calmodulin-dependent protein kinase in rat brain. *J. Neurosci.* **5**, 3270–3277 (1985).